LONG-TERM STREAMFLOW SENSITIVITY TO RAINFALL VARIABILITY UNDER IPCC SRES CLIMATE CHANGE SCENARIO

Boosik Kang[1] and Jorge A. Ramírez[2]

[1] Hydrosystems Engineering Center, Korea Water Resources Corporation, Daejeon, Korea
[2] Department of Civil Engineering, Colorado State University, Ft. Collins, CO, USA

Abstract: Long term streamflow regime under virtual climate change scenario was examined. Rainfall forecast simulation of the Canadian Global Coupled Model (CGCM2) of the Canadian Climate Center for modeling and analysis for the IPCC SRES B2 scenario was used for analysis. The B2 scenario envisions slower population growth (10.4 billion by 2010) with a more rapidly evolving economy and more emphasis on environmental protection. The relatively large scale of GCM hinders the accurate computation of the important streamflow characteristics such as the peak flow rate and lag time, etc. The GCM rainfall with more than 100km scale was downscaled to 2km-scale using the space-time stochastic random cascade model. The HEC-HMS was used for distributed hydrologic model which can take the grid rainfall as input data. The result illustrates that the annual variation of the total runoff and the peak flow can be much greater than rainfall variation, which means actual impact of rainfall variation for the available water resources can be much greater than the extent of the rainfall variation.

Keywords: GCM; climate change; long-term streamflow; downscaling

1. INTRODUCTION

The recent unusual extreme events of floods and droughts are reported to be attributed by climate change. There have been a lot of researches on global climate change and the increase of the GHG (Green House Gases) will bring about the global warming. However, the GHG's effects on the global movement of moisture and distribution of precipitation still be a challenging problem. GCMs give quantitative values of precipitation under virtual conditions of climate change, even though its use in for predicting the regional phenomena should be very careful. Before hydrologists can figure out the accurate amount of rainfall and its variability enough in the future, they first need to examine how the streamflow regime, e.g. total streamflow or peakflow is affected by rainfall variability.

Assessing the impacts of climate variability and change on hydrologic response and water resources under global climate change conditions has drawn attention of scientists since '90s (e.g., Epstein and Ramirez, 1994; Kite et al., 1994; Miller et al., 1994; Mohseni and Stefan 1998; Olivera et al., 2000; Arora and Boer, 2001). Even though some of the models use

distributed precipitation, they are based on limited number of ground observations. Downscaling the GCM precipitation was attained by multi-season, multi-site disaggregation method based on ground observation (Epstein and Ramírez, 1994; Kite et al., 1994) or multiple regression based on geographical coordinates and elevation (Yao and Terakawa, 1999).

In their work, Epstein and Ramírez (1994) applied daily spatial disaggregation techniques to the downscaling problem for the upper Rio Grande basin in Colorado. Their spatial disaggregation models were used to downscale Canadian Climate Centre GCM temperature and precipitation regimes to site specific locations within the study basin, preserving spatial covariance structures at all spatial scales. They used the Precipitation Runoff Modeling System (PRMS), a deterministic rainfall runoff model to examine hydrologic sensitivity under the disaggregated climate forcing. Under a doubled CO_2 scenario, an average 3.5 °C in disaggregated GCM temperature and a slight (less than 1.5%) decrease in disaggregated GCM annual precipitation result in significant snowpack accumulation decreases. Peak pack water equivalent decreases as large as 35% are observed. Total annual runoff decreases by an average of 17.7%, increasing during the fall and winter and decreasing in spring and summer. A seasonal shift towards earlier in the year is observed in peak runoff, soil moisture storage and evapotranspiration. Soil moisture increases during winter months and decreases during summer. Evapotranspiration closely follows soil moisture in all seasonal changes.

Kite, et al. (1994) carried out streamflow simulations for the Mackenzie River basin ($1.6\times10^6 km^2$) using the climatological outputs from the CCC GCMII. The operating scales of CCC GCMII were 3.75° and 20 minutes. One GCM pixel covers $72{,}000-92{,}000 km^2$ of area which varies depending on latitude. They used simple lumped reservoir parametric (SLURP) distributed watershed model that is similar to the macro-scale water balance model. They subdivided the entire watershed into 5 grouped response units (GRU). Within each GRU, the water balance components of evaporation, overland flow, infiltration and groundwater flow were calculated. The hydrograph at GRU's outlet is obtained considering the travel time between each pixel and basin outlet. Eventually the hydrograph at the main outlet of the basin is calculated from channel routing using non-linear storage function. This model is a distributed model only in the sense that the hydrologic parameters are associated with the distribution of land covers. GCM calculates excess water and soil moisture at the land surface on the basis of the vertical water balance between precipitation, surface evaporation, and the water holding capacity of the soil. In GCMs, the precipitation and surface evaporation are mainly driven by heat and energy dynamics, and tracking lateral, gravity driven flow, like streamflow, is simplified or not considered.

The approach to incorporate meteorological model simulation for predicting streamflow was taken by Yu, et al(1999). They simulated the river basin response to single-storm events by linking HEC-HMS (Hydrologic Modeling System) to the Penn State-NCAR Mesoscale Meteorological Model (MM5) with 3 nested domains. The dynamical downscaling was implemented from a scale of $36\,km$ to a scale of $4\,km$ through triple nesting. Using the distributed precipitation obtained from the dynamical downscaling to drive a distributed watershed model was a notable advance over former methodolo-

gies. Their study area is the Upper West Branch of the Susquehanna River Basin ($14{,}710\,km^2$). However, their downscaled precipitation shows significant over- or under estimation of the peaks. When considering that the hydrologic model employs a 10-min time step, those differences in temporal evolution of rainfall hyetographs can produce undesirable results in the runoff hydrograph. A similar methodology is employed here, except that the downscaling procedure is based on a random cascade model as opposed to a dynamical model.

Yao and Terakawa (1999)'s research was another example of coupling distributed hydrologic model with distributed grid rainfall. They developed a distributed hydrological model for the basin divided into 1 km -scale squared meshes. The mesh-based precipitation was obtained from gage observations through downscaling using a stepwise regression method. The monthly precipitation is regressed in terms of latitude, longitude, elevation, and the precipitation of the reference location. The monthly regression formula with same coefficients is applied for day of each month with stepwise manner. This downscaling method is straightforward and effective for a watershed that is small enough so that the precipitation of the specific location is highly correlated to that of the reference location. Its main shortcomings are that: a) accuracy decreases as the point of interest moves away from the reference gage station and b) spatial intermittency in the spatial coverage of precipitation cannot be properly simulated. Therefore, the daily runoff in periods of low flow tends to be underestimated.

Generally, in large-scale watersheds, parameters associated with wave celerity and hydraulic geometry, which are required for distributed dynamic routing, cannot be determined easily. Therefore, simple semi-distributed approaches have been preferred instead. In existing large-scale watershed models, the monthly hydrograph is relatively well simulated (e.g., Kite, et al., 1994 and Yao and Terakawa, 1999). Typically, these models use simple interpolation methods (e.g., Thiessen polygons, simple regression, Kriging, etc.) for spatial precipitation description and simulation. For the case of daily runoff, the hydrograph can be fitted to observation through parameter calibration. However, the calibrated parameters cannot always produce accurate hydrograph for precipitation other than what is used for calibration. That is truer for larger-scale watershed models. Runoff tends to be underestimated for uniformly distributed precipitation that does not consider spatial variability. Therefore, as the size of the computational time step decreases, the ability to characterize and account for the spatial variability increases in importance for an accurate simulation of hydrological response.

In this paper we show that, under plausible virtual climate change scenarios, the variability of total streamflow and peak flow can be much greater than the variability of precipitation itself. This can be interpreted as implying that the impact of climate change on streamflow can be more severe than can be expected from the rainfall pattern.

2. STUDY AREA

The South Platte River basin is located in the southwest corner of the Missouri River Basin. It lies between the latitudes $101°$ and $107°$ and between the longitudes $38°$ and $42°$ in the states of Colorado, Wyoming and Nebraska. The basin is enclosed by the Continental Divide on the west, the North Platte River Basin to the north, the Arkansas River Basin to the south, the

Republican River Basin to the southeast and the Lower Platte River Basin to the east. Figure 1 shows a synoptic view and longitudinal river profile of the South Platte watershed. The total basin area is 62,936 km^2, which makes up 4.6% of the total drainage area of the Missouri River. The longest flow length is about 711 km.

According to the classification of the USGS, the South Platte River basin is a part of the Missouri region and consists of 19 sub-basins. Among these, the Headwaters basin (HUC #10190001) is located at most upstream of the South Platte River (Figure 1) and virgin flow is relatively well preserved. The hydrologic analysis presented in this study was performed for the Headwaters basin (HUC #10190001). The outlet of the Headwaters basin corresponds to the streamflow gaging station of the South Platte River near Lake George (USGS06696000), which is located at Park County, Colorado, 38°54'19" in latitude and 105°28'22" in longitude. The drainage area of HUC #10190001 is 2,465 km^2 and the datum of the gage is 2,578m above sea level.

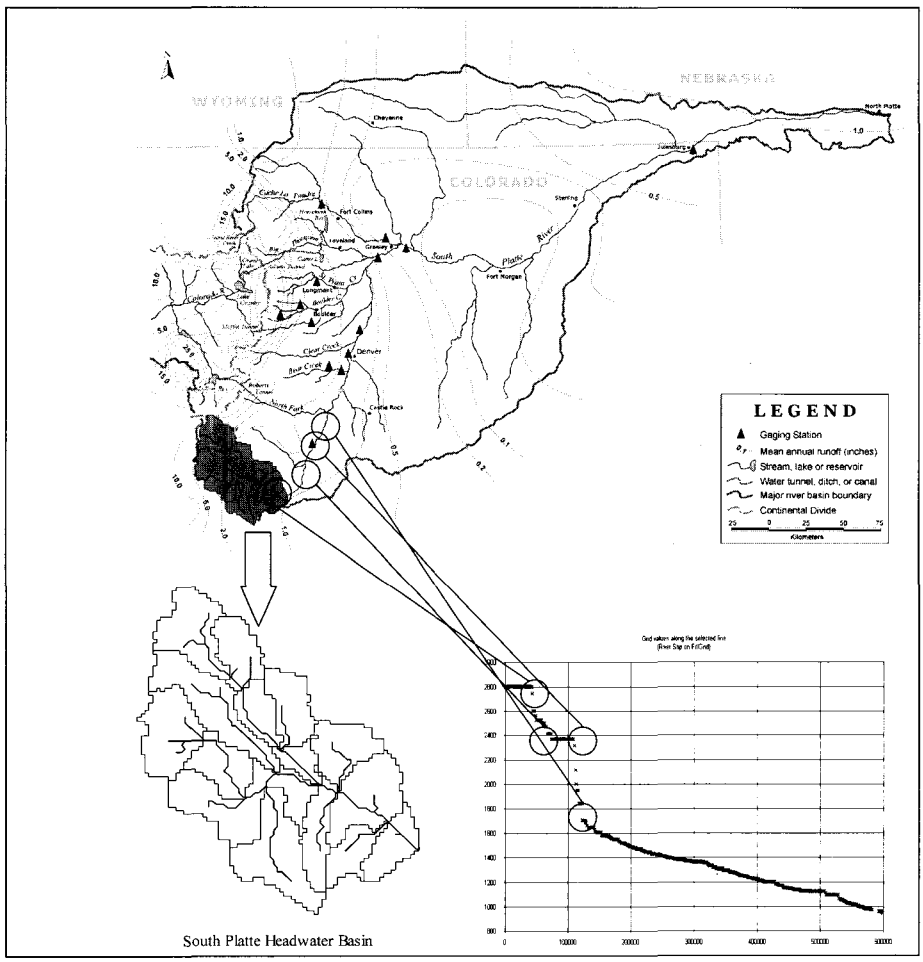

Figure 1. Synoptic view and longitudinal river profile of South Platte Watershed

3. GCM AND CLIMATE CHANGE SCENARIO

This study uses output from the CGCM2 model of the Canadian Climate Center for modeling and analysis (CCCma) and its time series plot for the average annual temperature is given in Figure 2. CGCM2 of CCCma is reported to be one of the most reliable GCM developed to date. The second version of the Canadian Global Coupled Model (CGCM2), is based on the earlier CGCM1, and improvements aimed at addressing shortcomings identified in the first version. In particular, the ocean mixing parameterization has been changed from horizontal/vertical diffusion scheme to the isopycnal/eddy stirring parameterization, and sea-ice dynamics has been included. In addition, other technical modifications were made in the ocean spin-up and flux adjustment procedure. A description of CGCM2 and a comparison, relative to CGCM1, of its response to increasing greenhouse-gas forcing can be found in Flato and Boer (2000).

IPCC SRES 'A2' and 'B2'

The CCCma employed 3 different scenarios: The IS92a scenario has effective CO concentration increasing at 1% per year after 1990. The IPCC IS92a scenario specifies equivalent greenhouse gas (GHG) concentrations and sulphate Aerosol loadings (GHG+A) from 1850 to 2100. The IPCC Special Report on Emission Scenarios (SRES) provides 40 different scenarios that are deemed *equally likely*. For the Third Assessment Report, the IPCC facilitated the conversion of two of these emission scenarios (A2 and B2) into concentration scenarios for use in climate simulations. The forcing changes implied by the concentrations were used to scale the equivalent CO_2 values to be consistent with the 1990 value in the IS92a simulation. The A2 scenario envisions population growth to 15 billion by the year 2100 and rather slow economic and technological development. It projects slightly lower GHG emissions than the IS92a scenario, but also slightly lower aerosol loadings, such that the warming response differs little from that of the earlier scenario. The B2 scenario envisions slower population growth (10.4 billion by 2100) with a more rapidly evolving economy and more emphasis on environmental protection. It therefore produces lower emissions and less future warming. Climate change results based on the A2 and B2 scenarios are also discussed in the IPCC Third Assessment Report. Because of the data availability, only IPCC SRES B2 scenario is used in this research. The B2 scenario produces less warming than the A2 or IS92a results. A total of 111 years of monthly data is available from the CCCma web site. However, daily data can be obtained through direct order. The data set for IPCC SRES B2 used in this study consist of 4 different time windows (1975-1995, 2011-2030, 2041-2060, 2071-2090). Figure 2 shows the increasing temperature trend of CGCM2 simulation for Central US and South Platte river basin. Because the South Platte river basin is located in the northwest section of the Central US, the time series for South Platte river is shifted lower about $2\,^{\circ}C$ from the time series of the Central US. Despite the significant shift in temperature, the rainfall pattern stays consistent. Figure 2 shows the average annual temperature simulated for the Central U.S. and for the South Platte watershed for the SRES B2 scenario.

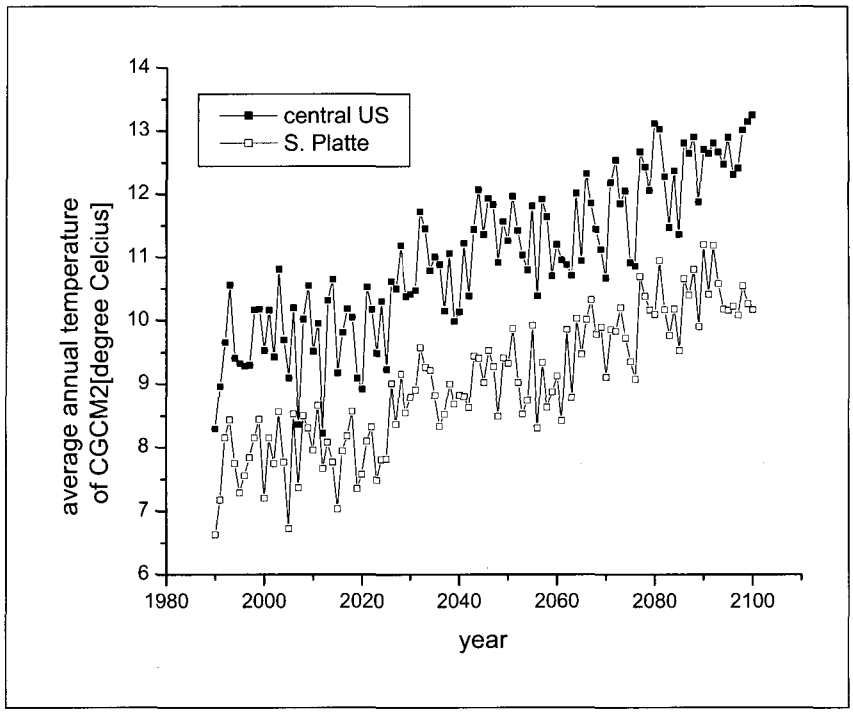

Figure 2. Average annual temperature of CGCM2 simulation

4. STREAMFLOW SIMULATIONS

4-1 Downscaling of GCM rainfall simulation

The most direct and straightforward way of downscaling (in the broad sense) is direct interpolation method. Direct interpolation method is easy to apply and could be effective for smoothly varying fields such as sea level pressure, but not appropriate for highly heterogeneous fields such as precipitation (Cohen and Allsopp, 1988). In the narrow sense, downscaling incorporates regional scale variability of the underlying region as well as the heterogeneity and nonlinearity governing the hydrological processes. Downscaling schemes can be classified into 2 general categories; physical process based techniques using nested models and mathematical (or statistical) based techniques using regression, nonlinear dynamics, Markov process or multiplicative random cascades. Wilby and Wigley (1997) classified the downscaling schemes more in detail into 4 categories, namely: regression methods, weather-pattern based approaches, stochastic weather generators, and limited-area modeling. Initially, 'Downscaling' schemes have emerged as a means of interpolating regional scale atmospheric predictor variables (such as a mean sea-level pressure, vorticity, etc.) to station-scale meteorological series (temperature, precipitation, etc.) (e.g., Kim et al., 1984; Klein, 1985; Wigley et al., 1990; Epstein and Ramirez, 1994). Mostly they used monthly mean and area averages (over $10^5 - 10^6 km^2$) as predictor variables, except for the work of Epstein and Ramírez (1994) for which daily values were used. One of the limita-

tions of the regression approach is that it can be useful if a strong relationship between a large-scale parameter and regional climate has been identified. Furthermore, as with many statistical tools, regression approaches could not be used beyond the range of the data used to fit the model. The statistical model is computationally economical but cannot include the local effect explicitly. In contrast, the nested method causes heavy computational burden but can include the local effect. Furthermore, atmospheric processes can be coupled with ecological and hydrological processes. Both methods depend critically on the quality of the large-scale flow field in GCMs. However, the parameters used in physical climate models are often derived from the data obtained in regional experiments, but the resulting approximations are then used everywhere on the globe. Clearly, this procedure yields less reliably simulated local values (von Storch et al., 1993). Marengo et al. (1994) also proposed that improved parameterization of spatially heterogeneous rainfall in each grid box should improve simulations of spatial and temporal variations of evaporation and runoff. However, this approach is still in development and requires not only detailed surface climate data but also high end computer capacity.

The Space-Time Stochastic Random Cascade Model (Kang and Ramirez, 2001 and 2002) used in this research is modified version of existing Multiplicative Random Cascade Model which was originally developed by Over and Gupta (1995). The main advantage of the Space-Time Stochastic Random Cascade Model is to reproduce the spatial clustering feature, spatial geometric gradient within cluster, inter-scale correlation structure and relatively low computational burden. The conceptual structure of the Space-Time Stochastic Random Cascade Model is shown in Figure 3.

4-2 Calibration of HEC-HMS

HEC-HMS is the GIS-based distributed rainfall-runoff model. The main advantage of the HEC-HMS is its capability to handle geo-spatial

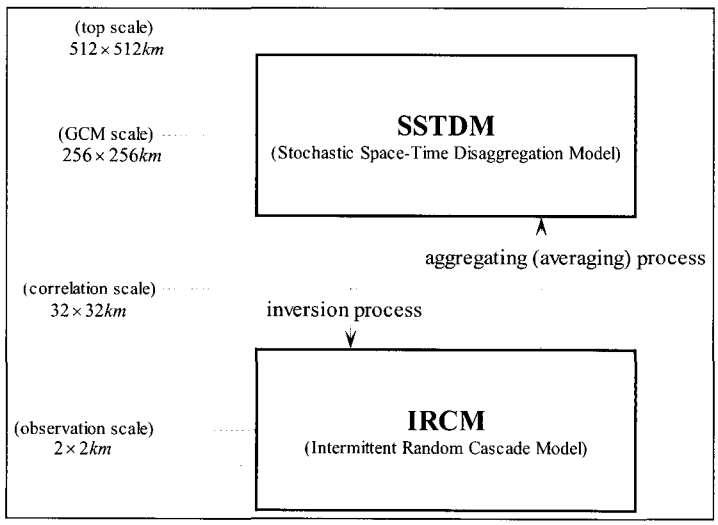

Figure 3. Conceptual structure of the Space-Time Stochastic Random Cascade Model

information and distributed grid-based precipitation data. Among the variety of specific options for routing methods, the gridded Soil Moisture Accounting (SMA), the ModClark quasi-distributed linear transform, baseflow recession, and Muskingum were selected for sub-basin loss method, sub-basin transform, baseflow, and channel routing, respectively. The sub-basin and channel configuration is shown in Figure 4. Even though the SMA model components represent the physical characteristics of the watershed, these parameters may or may not be directly correlated with measured or observed physical properties. That is because the SMA algorithm applies some extent of lumping to its parameters in approximating the combined physical characteristics for a given watershed. The final calibration of the HMS model to the 1997 JJA(June-July-August) NEXRAD precipitation and the hydrograph for daily streamflow at the outlet of the basin (S. Platte River near Lake George) are shown in Table 1 ~4 and Figure 4, respectively.

Table 1. Calibrated parameters of HMS model (Initial storage)

Initial storage					
Sub-basin	Canopy	Surface	Soil profile	Groundwater1	Groundwater2
R100W50	20	50	70	100	100
R170W150	20	50	70	100	100
R230W200	20	50	70	100	100
R270W250	20	50	70	100	100
R310W310	20	50	70	100	100
R220W220	20	50	70	100	100
R240W240	20	50	70	100	100
R470W420	20	50	70	100	100
R410W380	20	50	70	100	100
R370W360	20	50	70	100	100
R300W300	20	50	70	100	100
R280W280	20	50	70	100	100
R520W500	10	30	50	100	100
R490W490	20	50	70	100	100
R400W400	20	50	70	100	100

Table 2. Calibrated parameters of HMS model (Soil Moisture Accounting units)

Soil Moisture Accounting units						
SMA unit	Canopy	Surface		Soil Profile		
	Storage capacity(mm)	Storage capacity(mm)	Soil Infiltration Max. Rate(mm/hr)	Storage capacity(mm)	Tension Zone capacity(mm)	Percolation Max. Rate(mm/hr)
R520W500	1	5	2	10	2	1

R470W420	2	7	2	15	4	3
R300W300	2	7	2	10	3	2
R100W50	2	5	2	5	2	1
R170W150	2	5	2	5	2	1
R400W400	1	1	1	3	2	0.5
R370W360	2	3	2	2	1	0.5
R280W280	2	5	2	5	2	0.5
R490W490	0.5	0.5	0.5	1.2	1	0.5
R230W200	1	2	1	3	1	0.5
R270W250	0.5	2	1	2	1	0.5
R310W310	0.5	0.5	0.5	2	1	0.5
R220W220	1	2	1	4	3	0.5
R240W240	2	5	2	5	2	1
R410W380	1	5	3	10	3	2

Soil Moisture Accounting units						
SMA unit	Groundwater1			Groundwater2		
	Storage capacity(mm)	Percolation Max. Rate(mm/hr)	Storage coefficient (hr)	Storage capac-ity(mm)	Percolation Max. Rate(mm/hr)	Storage coefficient (hr)
R520W500	20	0.5	30	40	0.5	50
R470W420	25	0.5	30	40	0.5	50
R300W300	20	0.5	30	40	0.5	50
R100W50	20	0.5	30	40	0.5	50
R170W150	20	0.5	30	40	0.5	50
R400W400	20	0.5	30	40	0.5	50
R370W360	15	0.5	30	40	0.5	50
R280W280	15	0.5	30	40	0.5	50
R490W490	10	0.5	30	40	0.5	50
R230W200	15	0.5	30	40	0.5	50
R270W250	10	0.5	30	40	0.5	50
R310W310	10	0.5	30	40	0.5	50
R220W220	15	0.5	30	40	0.5	50
R240W240	20	0.5	30	40	0.5	50
R410W380	20	0.5	30	40	0.5	50

Table 3. Calibrated parameters of HMS model (ModClark transform & Groundwater recession)

	ModClark transform		Groundwater recession		
Sub-basin	Time of Concentration (hrs)	Storage Coefficient (hrs)	Initial Flow (cms)	Recession Ratio	Threshhold Flow (cms)
R100W50	40	150	0.1	0.99	2
R170W150	20	130	0.1	0.99	2
R230W200	40	120	0.1	0.92	2
R270W250	60	150	0.5	0.99	2
R310W310	40	110	0.1	0.99	2
R220W220	40	80	0.1	0.94	2
R240W240	40	80	0.1	0.90	2
R470W420	120	150	0.1	0.8	2
R410W380	65	120	0.1	0.85	2
R370W360	100	120	0.1	0.99	2
R300W300	120	150	0.1	0.8	2
R280W280	80	120	0.1	0.85	2
R520W500	150	140	0.1	0.9	2
R490W490	100	150	0.1	0.98	2
R400W400	60	100	0.1	0.995	2

Table 4. Calibrated parameters of HMS model (Muskingum channel routing)

	Muskingum channel routing		
Reach	K (hrs)	X	Number of sub-reaches
R170	2	0.2	1
R220	6	0.2	1
R360	8	0.2	1
R370	25	0.2	1
R310	5	0.2	1
R380	10	0.2	1
R410	2	0.2	1
R280	10	0.2	1
R390	12	0.2	1
R420	35	0.2	1
R470	20	0.2	1
R500	20	0.2	1
R520	25	0.2	1

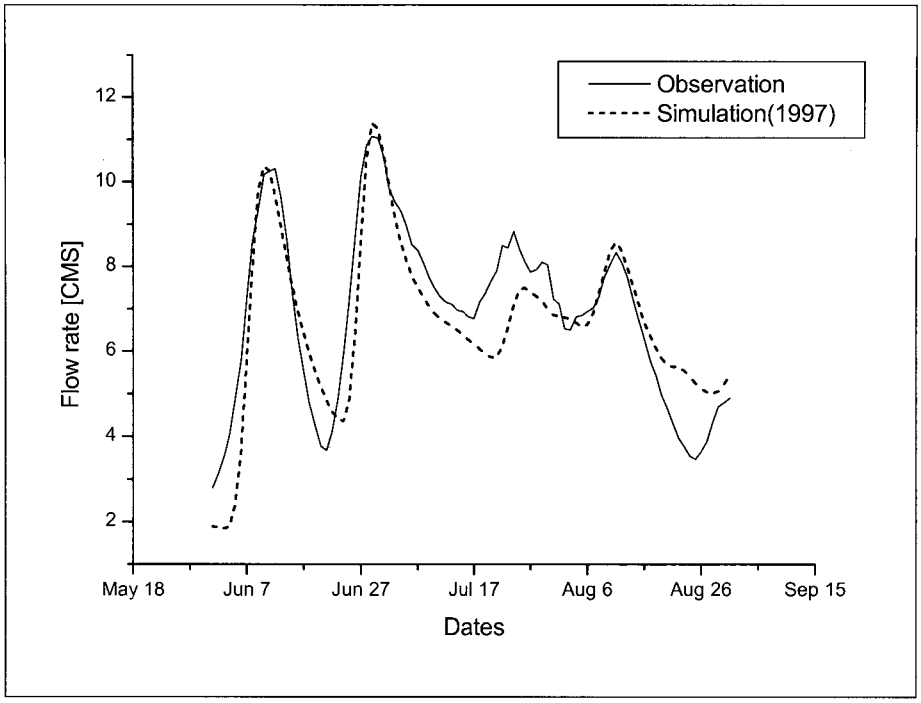

Figure 4. The hydrograph at the outlet of Headwaters basin

4-3 Streamflow scenario analysis

Before proceeding to the streamflow prediction using GCM precipitation, the annual pattern of GCM precipitation is compared to the historical records of gage observations of the South Platte River basin.

When setting up climate change scenarios for GCM, from 1990 onward, an increase of 1% or less per year (it varies with the specific scenario) of the equivalent CO_2 is assumed. Based on this assumption, climate models constantly project an increase in global mean precipitation of between 3 to 15% for a temperature increase of 1.5 to 3.5 $^{\circ}C$. But these global average changes hide significant differences in regional precipitation patterns. Some large areas with increases or decreases in precipitation may have areas where precipitation changes in opposite direction (WSAT, 2000). Figure 3 shows that there is significant inconsistency between absolute values of GCM precipitation and historical records of gage observation. Nevertheless the relative variability in GCM precipitation can be respected. During 1990 to 2000, the climate conditions for running model are similar to those for the precipitation observations, but the model simulation value shows bias from the observation which needs to be adjusted. Therefore, the GCM precipitation needs to be adjusted to the local region by shifting the whole series by the difference or amount of bias between GCM precipitation and gage observation in 1990 to 2000 (Figure 5).

The HEC-HMC model developed by the U.S. Army Corps of Engineers was used for the distributed rainfall-runoff model and the GIS preprocessing was performed using HEC-GeoHMS. The grid (i.e., NEXRAD or GCM) precipitation

was used as an input to the HMS. In HMS, the gridded Soil Moisture Accounting scheme (SMA) was selected for calculating sub-basin losses, and the ModClark quasi-distributed linear transform method was applied in combination with the gridded SMA. Baseflow was computed using the exponential recession constant method. Finally, channel routing was performed using the Muskingum method. The 30-arc seconds GTOPO30 DEM data were used for terrain processing. The STATSGO of USDA Natural Resources Conservation Service was used for extracting soil geographic information.

In order to predict streamflows from GCM precipitation, the CCCma simulation is first downscaled using the space-time stochastic random cascade model (Kang & Ramirez, 2001 and 2002). Then, with the parameters used in the downscaling model calibrated with NEXRAD rainfall in 1997 (Kang & Ramirez, 2002), the hydrographs were produced for the CCCma scenarios. We did streamflow prediction for 2 temporal windows (2011-2020 and 2081-2090) of GCM precipitation. For each year, 10 hydrographs were simulated for 10 different spatial distributions of precipitation that are assumed to have common large-scale forcing (total precipitation). Therefore, 200 hydrographs were computed for the year 2011 to 2020 and 2081 to 2090. Because each of the 10 hydrograph simulations of a specific year has the same temporal distribution of rainfall, they have similar shapes (e.g., time to peak). However, the magnitude of total runoff or peak flow varies according to the spatial distribution of the rain fields. Figure 6 compares the coefficient of variation of the peak flows and runoff volumes and illustrates that the coefficient of variation of peak flow is higher than that of runoff volumes over most of the years. That means the distribution of peak flow rate is more scattered over the simulations and more sensitive to the spatial variability of rainfall than total runoff volume.

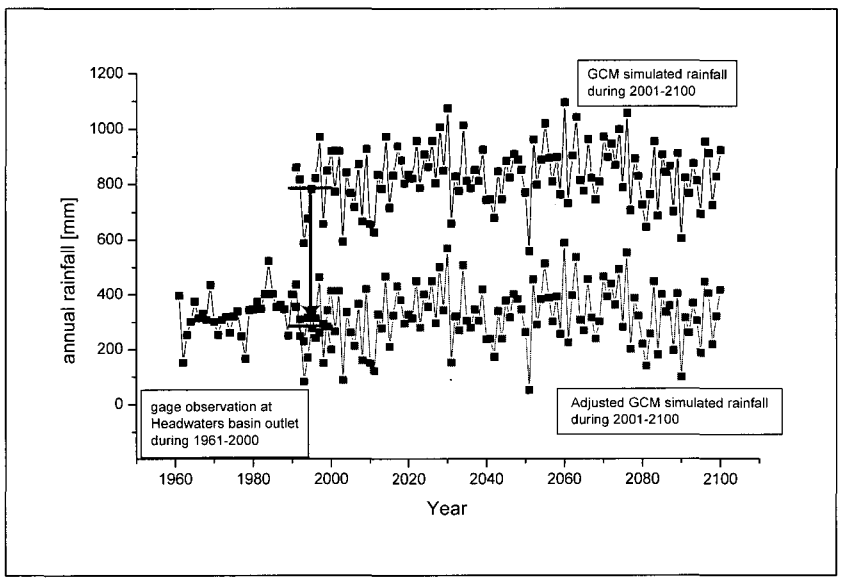

Figure 5. The comparison of GCM rainfall and historical observation of gage rainfall

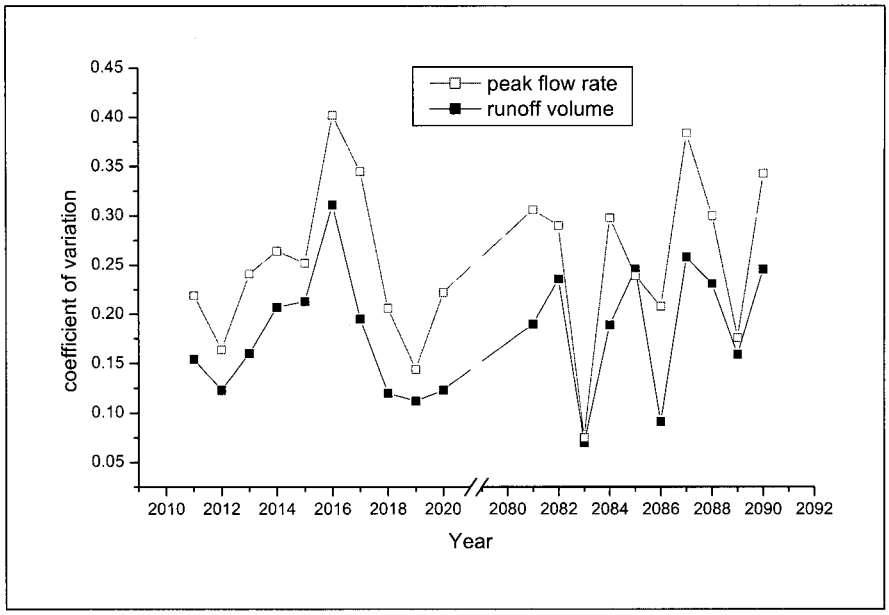

Figure 6. The coefficient of variation of the GCM hydrograph prediction

Figures 7 and 8 show the statistics of the simulated GCM precipitation and evaporation for 2 temporal windows of the data set. The comparison is made for annual values and JJA (June-July-August) values. These figures show that the annual evaporation is increased 4.65% due to temperature increases, whereas the average annual precipitation is not changed significantly. The JJA evaporation is increased 4.19%, whereas the JJA precipitation is decreased 4.2%, which results in the reduction of streamflow runoff in the latter 10 years. Figure 9 and 10 illustrate the trend shift in JJA runoff volume and peak flow rate corresponding to the GCM climate change scenarios. The JJA runoff volume is decreased 15.37% and the JJA peak flow rate is decreased 18.01%. Much of these reductions are the result of the decrease of JJA precipitation and the increase of JJA evaporation and those decreasing rates are much greater than the decreasing rate of precipitation. It is expected that the temporal variability of rainfall would affect the streamflow pattern. The peak flow and runoff volume have higher COV than JJA precipitation, and between peak flow and runoff volume, the peak flow has higher COV. Those results can be disadvantageous for water resources management. Even though the computation gives the quantitative values for the precipitation, total runoff volume and peak flow, the judgment for the consistency or decreasing/increasing trend should be very careful because of the relatively large standard deviations and a lot of uncertainties in the computational procedure. However, brief statistical tests will be shown in the next section for examining the significancy of long-term trends.

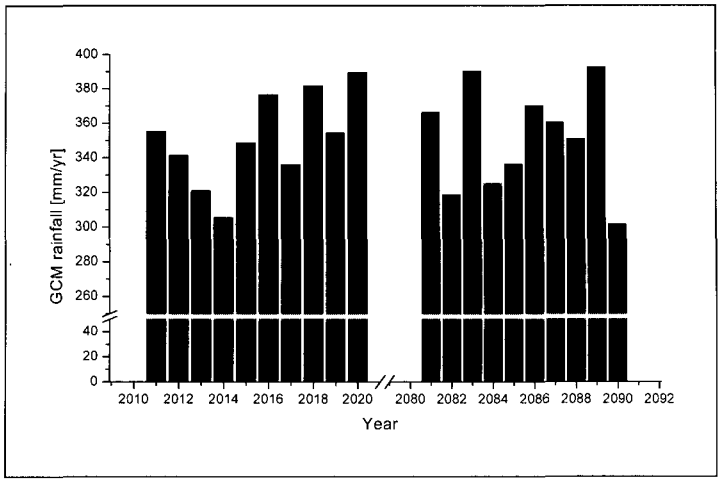

	2011~2020	2081~2090	
Mean	350.9 mm/yr	351.1 mm/yr	+0.06%
Standard deviation	26.7 mm/yr	30.4 mm/yr	+14.1%
Coeff. of Variation	0.076	0.087	+14.5%

annual precipitation

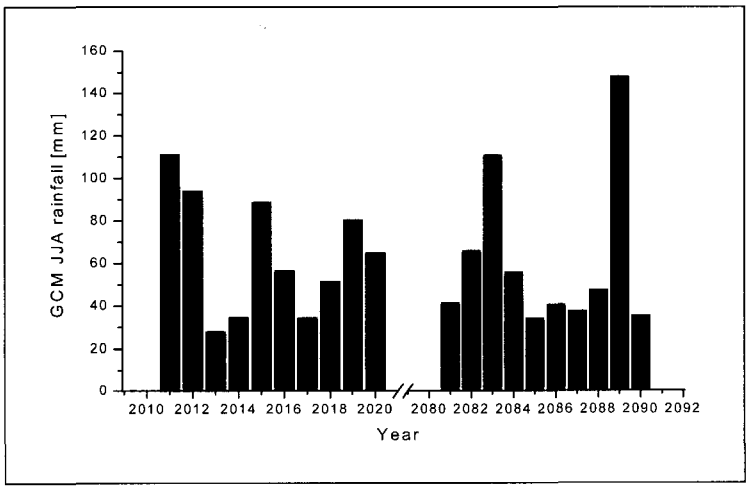

	2011~2020	2081~2090	
Mean	64.4	61.7	-4.2%
Standard deviation	28.4	38.1	+33.9%
Coeff. of Variation	0.441	0.618	+40.0%

JJA precipitation

Figure 7. The time series of GCM rainfall simulation data set for South Platte Headwaters Basin

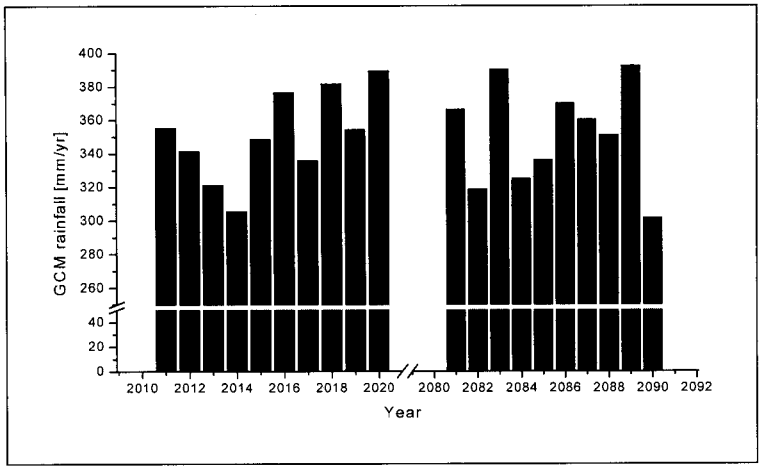

	2011~2020	2081~2090	
Mean	304.3 mm/yr	318.5 mm/yr	+4.65%
Standard deviation	13.0 mm/yr	16.7 mm/yr	+28.2%
Coeff. of Variation	0.076	0.087	+14.5%

annual evaporation

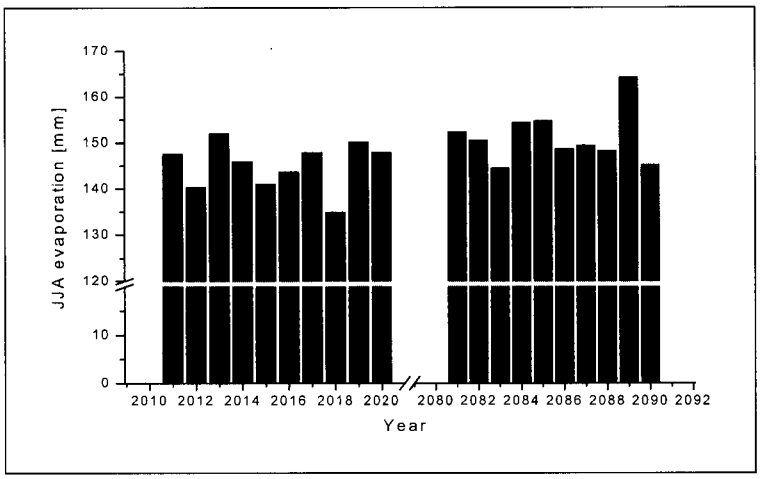

	2011~2020	2081~2090	
Mean	145.0	151.2	+4.19%
Standard deviation	5.2	5.7	+10.4%
Coeff. of Variation	0.036	0.038	+5.56%

JJA evaporation

Figure 8. The time series of GCM evaporation simulation data set for South Platte Headwaters Basin

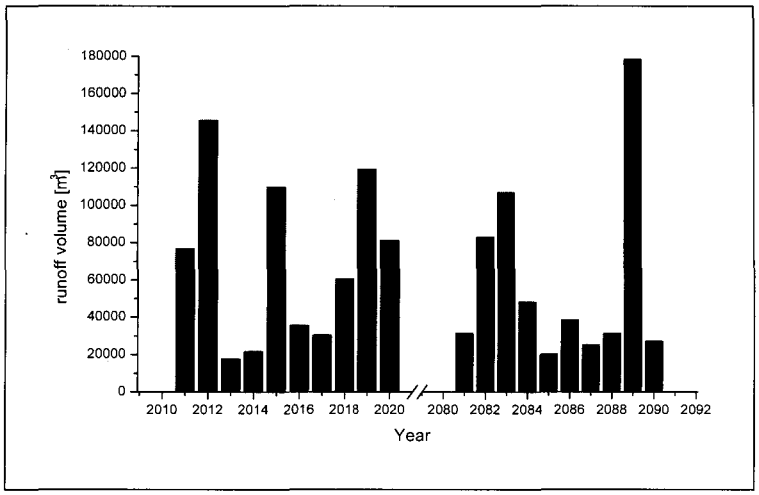

	2011~2020	2081~2090	
Mean	70,092.22m³	59,321.01m³	-15.37%
Standard deviation	44,476.9m³	50,391.0m³	+13.3%
Coeff. of Variation	0.635	0.849	+33.7%

Figure 9. The runoff volume for the GCM rainfall simulation data set

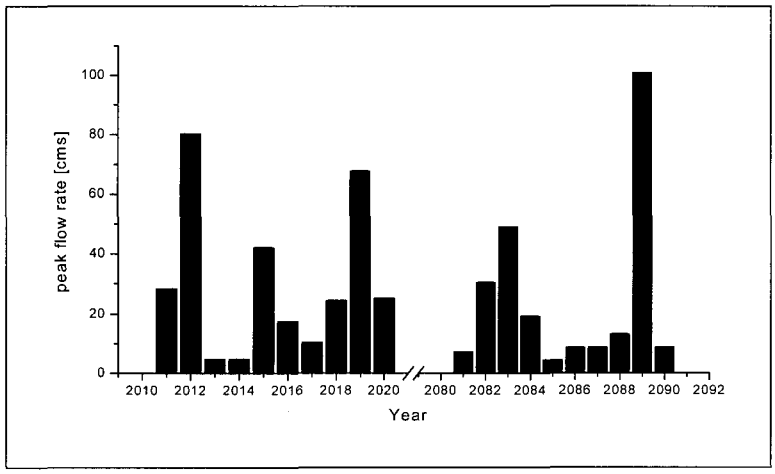

	2011~2020	2081~2090	
Mean	30.53cms	25.03cms	-18.01%
Standard deviation	25.7cms	29.9cms	+16.3%
Coeff. of Variation	0.842	1.195	+41.9%

Figure 10. The peak flow rate for the GCM rainfall simulation data set

5. STATISTICAL TESTS FOR THE RESULTS

The *null hypothesis* of no difference in the means between the first and the last 10-year periods considered is examined. However, because the variance cannot be assumed to remain constant between the 2 periods, the statistical test must explicitly account for a time-varying variance (Kottegoda and Rosso, 1997). When the variances are unequal, the statistic does not have a t-distribution. This is called the Behrens-Fisher problem. In case of observations taken from normal populations with unknown and unequal variances, the statistic has an approxi

$$T = \frac{(\overline{X}_1 - \overline{X}_2) - (\mu_1 - \mu_2)}{\sqrt{\left(S_1^{\,2}/n_1\right) + \left(S_2^{\,2}/n_2\right)}}$$

$$\nu = \frac{\left[\left(\hat{S}_1^{\,2}/n_1\right) + \left(\hat{S}_2^{\,2}/n_2\right)\right]^2}{\left[\left(\hat{S}_1^{\,2}/n_1\right)^2/(n_1-1)\right] + \left[\left(\hat{S}_2^{\,2}/n_2\right)^2/(n_2-1)\right]}$$

matet distribution with degrees of freedom.

The result of the test for the null hypothesis for JJA rainfall, runoff volumes, and peak flow rate is given in the Table 5 in which there are not significant proofs of changing trends. However, Figure 9 & 10 shows that the values in 2089 are extraordinarily high and they can be taken as outlier. The basic statisitics for the test without the outliers are in the Table 6～8. Table 9 shows that the null hypotheses except for JJA rainfall were rejected. So, one can tell the runoff volume and the peak discharge would decrease with level of significance $\alpha = 0.1$. Even though the null hypothesis of JJA rainfall was not rejected when $\alpha = 0.1$, it can be rejected if $\alpha \approx 0.16$.

Table 5. Test of null hypothesis with the original data

	JJA rainfall	Runoff volume	Peak flow rate
ν	17	18	18
T	0.179	0.507	0.440
F at $\alpha = 0.1$	1.333	1.330	1.330
Null hypothesis	Not rejected	Not rejected	Not rejected

Table 6. Basic statistics of JJA precipitation without outlier

	2011～2020	2081～2090	
Mean	64.4	52.1	- 19.1%
Standard deviation	28.4	24.3	- 14.3%
C.O.V	0.441	0.466	+ 5.36%

Table 7. Basic statistics of runoff volumes without outlier

	2011～2020	2081～2090	
Mean	70,092.22㎥	46,053.13㎥	- 34.3%
Standard deviation	44,476.9㎥	29,601.41㎥	- 33.45%
C.O.V	0.635	0.643	1.24%

Table 8. Basic statistics of peak flow rate without outlier

	2011~2020	2081~2090	
Mean	30.53cms	16.61cms	- 45.61%
Standard deviation	25.7cms	14.51cms	- 43.65%
C.O.V	0.842	0.874	3.66%

Table 9. Basic statistics of JJA precipitation without outlier

	JJA rainfall	Runoff volume	Peak flow rate
ν	18	16	14
T	1.038	1.423	1.490
F at $\alpha = 0.1$	1.330	1.330	1.330
Null hypothesis	Not rejected	Rejected	Rejected

As indicated above, these results have large inherent uncertainty as a result of the uncertainty in each of the models used, namely, the GCM model, the downscaling model, and the HEC-HMS model. In addition, so-called "the deterministic chaos" is known to be important reason for hindering deterministic long-term climate forecasting. However, we need to pay attention to the relative correlation between the meteorologic (precipitation) and the hydrologic (streamflow) phenomena.

6. CONCLUSIONS

The long-term relationship between the rainfall variability and streamflow regime was examined. The result shows that the annual variation of the total runoff and the peak flow can be much greater than rainfall variation, which means actual impact of rainfall variation for the available water resources can be much greater than the extent of rainfall variation. Even though under the climate change scenario and the model used in this research did not produce significant increase in rainfall variability, other scenario in other models or actual phenomenon could be opposite. More reliable analysis will be expected with more reliable data and advanced models in the future.

REFERENCES

Arora, V.K. and G.J. Boer, 2001: Effects of Simulated Climate Change on the Hydrology of Major River Basins, J. of Geophys. Res., 104(D12), 3335-3348

Cohen, S. J. and T. R. Allsopp, 1988: The Potential Impacts of a Scenario of CO_2-induced Climatic Change on Ontario, Canada, *J. of Climate*, 1, 669-681

Epstein, D., and J. A. Ramírez, 1993: A Statistical Climate Inversion Scheme and its Application in Hydrologic Impact Assessment Studies Associated with Global Climate Variability. *Proceedings Third International Symposium on Engineering Hydrology*. ASCE Conference, San Francisco, C. Y. Kuo Ed., pp. 61-66.

Flato, G.M. and G.J. Boer, 2001: Warming Asymmetry in Climate Change Simulations,

Geophys. Res. Lett., 28, 195-198.

Kang, B. and J.A. Ramirez, 2002: Stochastic Space-Time Downscaling for GCM Precipitation, *2002 American Geophysical Meeting (AGU) Spring Meeting*, May 28-31, Washington, D.C.

Kang, B. and J. A. Ramirez, 2001: Comparative study of the statistical features of random cascade models for spatial rainfall downscaling, *Proceedings AGU Hydrology Days 2001*, J. A. Ramirez Ed., Hydrology Days Publications, Fort Collins, CO. pp 151-164.

Kite, G.W., A. Dalton, and K. Dion, 1994: Simulation of Streamflow in a Macroscale Watershed Using General Circulation Model Data, *Water Resources Research*, 34(5), 1287-1298

Kim, J.-W., J.-T. Chang, N. L. Baker, D. S. Wilks, and W. L. Gates, 1984: The Statistical Problem of Climate Inversion: Determination of the Relationship between Local and Large-Scale Climate. *Monthly Weather Review*, 112, 2069 - 2077.

Kottegoda, N.T. and R. Rosso, 1997: Statistics, Probability, and Reliability for Civil and Environmental Engineers, pp. 264, McGraw-Hill

Marengo, J.A., et al., 1994: Calculations of River-Runoff in the GISS GCM: Impact of a New Land-Surface Parameterization and Runoff Routing Model on the Hydrology of the Amazon River, *Climate Dynamics*, 10, 349-361,

Miller, J.R., G.L. Russell, and G. Caliri, 1994: Continental Scale River Flow in Climate Models, *J. of Climate*, 7, 914-928

Moseni, O. and H.G. Stefan, 1998: A Monthly Streamflow Model, *Water Resources Research*, 34(5), 1287-1298

Olivera, F., J. Famiglietti, and K, Asante, 2000: Global-scale Flow Routing Using a Source-to-sink Algorithm, *Water Resources Research*, 36(8), 2197-2207

Over, T.M., and V.J. Gupta, 1996: A Space-Time Theory of Mesoscale Rainfall using Random Cascades, *J. of Geophy. Res.*, 101(D21), 26319-26331

WSAT, 2000: Water: The potential Consequences of Climate Variability and Change for the Water Resources of the United States, The Report of the Water Sector Assessment Team of the National Assessment of the Potential Consequences, For the U.S. Global Change Research Program.

Wigley, T. M. L., P. D. Jones, K. R. Briffa, and G. Smith, 1990: Obtaining Sub-Grid-Scale Information From Coarse Resolution General Circulation Model Output. *Journal of Geophysical Research.* 95(D2), 1943 - 1953.

Wilby, R.L. and T.M.L. Wigley, 1997: Downscaling General Circulation Model output: A review of methods and limitations, *Progress in Physical Geography*, 21(4), 530-548.

Yao, H., and A. Terakawa, 1999: Distributed Hydrological Model for Fuji River Basin, *J. of Hydrologic Engineering*, 4(2), 108-116

Yu, Z., M.N. Lakhtakia, B. Yarnal, R.A. White, D.A. Miller, B. Frakes, E.J. Barron, C. Duffy and F.W. Schwartz, 1999: Simulating the River Basin Response to Atmospheric Forcing by Linking a Mesoscale Meteorologic Model and Hydrologic Model System, *J. of Hydrology*, 218, 72-91

Hydrosystems Engineering Center, Korea Water Resources Corporation, Daejeon, Korea
(E-mail: bskang@koreamail.co.kr)

Department of Civil Engineering, Colorado State University, Ft. Collins, CO, USA
(E-mail: ramirez@engr.colostate.edu)